

## Quantitative study of localization effects and recombination dynamics in GaAsBi/GaAs single quantum wells

M. K. Shakfa, D. Kalincev, X. Lu, S. R. Johnson, D. A. Beaton, T. Tiedje, A. Chernikov, S. Chatterjee, and M. Koch

Citation: *Journal of Applied Physics* **114**, 164306 (2013); doi: 10.1063/1.4826621

View online: <http://dx.doi.org/10.1063/1.4826621>

View Table of Contents: <http://scitation.aip.org/content/aip/journal/jap/114/16?ver=pdfcov>

Published by the [AIP Publishing](#)

---

### Articles you may be interested in

[Recombination kinetics of photogenerated electrons in InGaAs/InP quantum wells](#)

*J. Appl. Phys.* **119**, 094301 (2016); 10.1063/1.4942854

[Carrier dynamics between delocalized and localized states in type-II GaAsSb/GaAs quantum wells](#)

*Appl. Phys. Lett.* **98**, 061910 (2011); 10.1063/1.3548544

[Dynamics of carrier recombination and localization in AlGaIn quantum wells studied by time-resolved transmission spectroscopy](#)

*Appl. Phys. Lett.* **95**, 091910 (2009); 10.1063/1.3222972

[Photoluminescence study of carrier dynamics and recombination in a strained InGaAsP/InP multiple-quantum-well structure](#)

*J. Appl. Phys.* **86**, 3391 (1999); 10.1063/1.371219

[Type II recombination and band offset determination in a tensile strained InGaAs quantum well](#)

*Appl. Phys. Lett.* **70**, 3257 (1997); 10.1063/1.119140

---

A promotional banner for AIP Applied Physics Reviews. The background is a dark blue gradient with a bright light source on the right, creating a lens flare effect. On the left, there is a small inset image of a book cover for 'AIP Applied Physics Reviews' featuring a diagram of a quantum well structure. The main text 'NEW Special Topic Sections' is in large, white, bold, sans-serif font. Below this, the text 'NOW ONLINE' is in yellow, followed by 'Lithium Niobate Properties and Applications: Reviews of Emerging Trends' in white. The AIP Applied Physics Reviews logo is in the bottom right corner.

**NEW Special Topic Sections**

**NOW ONLINE**  
Lithium Niobate Properties and Applications:  
Reviews of Emerging Trends

**AIP** Applied Physics  
Reviews

## Quantitative study of localization effects and recombination dynamics in GaAsBi/GaAs single quantum wells

M. K. Shakfa,<sup>1,a)</sup> D. Kalincev,<sup>1</sup> X. Lu,<sup>2</sup> S. R. Johnson,<sup>2</sup> D. A. Beaton,<sup>3</sup> T. Tiedje,<sup>4</sup> A. Chernikov,<sup>1</sup> S. Chatterjee,<sup>1</sup> and M. Koch<sup>1</sup>

<sup>1</sup>*Department of Physics and Materials Sciences Center, Philipps-University of Marburg, Renthof 5, D-35032 Marburg, Germany*

<sup>2</sup>*Department of Electrical Engineering, Arizona State University, Tempe, Arizona 85287-6206, USA*

<sup>3</sup>*Department of Physics and Astronomy, University of British Columbia, Vancouver, British Columbia V6T 1Z4, Canada*

<sup>4</sup>*Department of Electrical and Computer Engineering, University of Victoria, Victoria, British Columbia V8W 3P6, Canada*

(Received 21 July 2013; accepted 7 October 2013; published online 23 October 2013)

Localization effects on the optical properties of GaAs<sub>1-x</sub>Bi<sub>x</sub>/GaAs single quantum wells (SQWs), with Bi contents ranging from  $x=1.1\%$  to  $6.0\%$ , are investigated using continuous-wave and time-resolved photoluminescence. The temperature- and excitation density dependence of the PL spectra are systematically studied, and the carrier recombination mechanisms are analyzed. At low temperatures, the time-integrated PL emission is dominated by the recombination of localized electron-hole pairs due to the varying content and clustering of Bi in the alloy. The extracted energy scales fluctuate tremendously when the Bi content is varied with a weak tendency to increase with Bi content. Relatively low energy scales are found for the SQW with  $x=5.5\%$ , which makes it a potential candidate for long-wavelength optoelectronic devices. © 2013 AIP Publishing LLC. [<http://dx.doi.org/10.1063/1.4826621>]

### I. INTRODUCTION

Bismuth containing semiconductor alloys such as GaAsBi have received much attention in recent years due to their unusual physical properties and potential application in long-wavelength optoelectronic and photonic devices.<sup>1-14</sup> A number of interesting observations are obtained by replacing a small percentage of As in GaAs with Bi, acting as an isoelectronic impurity. GaAsBi exhibits a large band gap bowing effect, resulting in a significant reduction of the band gap energy.<sup>1</sup> This behavior is typically explained using the valence-band anti-crossing model based on the coupling between the localized Bi states and the valence band of GaAs.<sup>2</sup> In addition, a large increase in the spin-orbit splitting makes GaAsBi promising for spintronic applications.<sup>3</sup> Furthermore, an increased carrier-phonon coupling due to the strong deformation of the GaAs lattice by comparably large Bi atoms is reported.<sup>4</sup> Otherwise, Bi incorporation into GaAs affects the carrier recombination processes strongly<sup>5</sup> due to the increasing density of the localized states. This leads to an extension of the band-edge toward lower energies, the so-called band-tail states.<sup>15</sup> The emergence of the localized states in GaAsBi is attributed to the fluctuations of the alloy composition together with the clustering of Bi.<sup>6</sup> Generally, the presence of localization effects within the material system leads to significant changes of carrier dynamics, thus affecting the performance of optoelectronic devices.

The ternary alloy GaAsBi was synthesized by metal organic chemical vapor deposition (MOCVD),<sup>7</sup> and by molecular beam epitaxy (MBE).<sup>8</sup> Quite recently, GaAsBi alloys have been achieved with the Bi content as high as

10.6%.<sup>9</sup> Moreover, GaAsBi/GaAs single- (SQW)<sup>10</sup> and multi-quantum-well (MQW)<sup>11</sup> structures have been reported. Photoluminescence (PL) spectroscopy is a useful tool to check the optical quality of semiconductor structures. Referring to the study mentioned at room temperature (RT) in Ref. 12, the PL intensity of the GaAsBi alloy is enhanced for high Bi contents up to 6.0% (4.5% in Ref. 9). This results from the more efficient confinement effects associated with the larger offset between GaAs and GaAsBi with increasing Bi content. Also, the localization effects near the valence band maximum increase with Bi content, thereby allowing a relatively efficient trapping process of holes, and thus a weak effect of the non-radiative centers on electron-hole pairs.<sup>9</sup> However, the PL intensity drops for larger Bi contents since the material quality degrades due to the increasing number of defects within the alloy structure. Besides, non-monotonous features in temperature dependent PL spectra of GaAsBi are observed by several groups.<sup>6,10,13</sup> This unusual behavior is successfully described using an excitonic hopping model based on two energy scales,<sup>6</sup> which are related to the above-mentioned disorder.

However, the influence of the Bi content on the localization energy scales and the carrier dynamics in the novel GaAs<sub>1-x</sub>Bi<sub>x</sub>/GaAs SQWs are not established so far. In the present work, continuous-wave (CW) and time-resolved PL (TRPL) techniques are employed to study the carrier dynamics and the optical properties of MBE grown GaAs<sub>1-x</sub>Bi<sub>x</sub>/GaAs SQWs. In particular, the temperature- and excitation density dependence of the PL peak energy, the PL linewidth (FWHM: full width at half maximum), the integrated PL intensity, and the PL decay time are investigated. The carrier recombination mechanisms are discussed. Furthermore, the impact of the Bi content on the localization effects is quantitatively analyzed.

<sup>a)</sup>Electronic mail: shakfa@staff.uni-marburg.de

## II. EXPERIMENTAL DETAILS

The samples studied in the present work are a set of  $\text{GaAs}_{1-x}\text{Bi}_x$  SQWs, epitaxially (MBE) grown on semi-insulating GaAs substrates with Bi contents of  $x = 1.1\%$ ,  $2.1\%$ ,  $5.5\%$ , and  $6.0\%$  at a growth rate of  $\sim 1\text{ nm/min}$ . The growth technique is described in Refs. 8 and 9. The structural quality is confirmed using high-resolution X-ray diffraction; these experiments including full dynamical simulations also independently corroborated the expected layer thicknesses and Bi contents. All samples consist of a  $300\text{ nm}$  GaAs buffer layer, followed by a QW layer and a  $20\text{ nm}$  GaAs cap layer. The QW widths range from  $12$  to  $14\text{ nm}$ . The growth parameters are summarized in Table I.

For the PL experiments the samples are mounted inside a liquid-helium-flow microscopy-cryostat, where the temperature is controlled between  $10\text{ K}$  and RT of  $292\text{ K}$ . The PL signal is collected normal to the sample surface in reflection geometry. CW- and TRPL measurements are performed. In the first case, the excitation source is a  $632.8\text{ nm}$  CW He-Ne laser. The PL emission is detected by an optical spectrum analyzer (OSA). TRPL measurements are carried out using a mode-locked Ti:sapphire laser tuned to  $780\text{ nm}$  with a repetition rate of  $80\text{ MHz}$  and a pulse duration of  $100\text{ fs}$ . The laser beam is focused on the sample down to a spot size of  $30\text{ }\mu\text{m}$  in diameter. The excitation density is about  $17.7\text{ MW/cm}^2$  for an average laser power of  $1\text{ mW}$ . A streak camera with an IR-sensitive cathode is used to detect the PL signal which is spectrally dispersed by an imaging spectrometer. The overall time resolution of the detection system is approximately  $10\text{ ps}$ . The spectral resolution in both CW and TR setups is  $1\text{ nm}$ .

## III. RESULTS AND DISCUSSION

In general, an interplay between recombination and relaxation processes of the carriers within disordered materials typically leads to a non-exponential decay of the PL.<sup>5,16–18</sup> Thus, in the following, the PL decay time is defined as the time required for the PL intensity to decrease to the fraction of  $\frac{1}{e}$  of its initial value. All of the TRPL spectra and PL transients are time- and spectrally integrated, respectively, over the complete detection window of  $2\text{ ns}$  and between  $0.95\text{ eV}$  and  $1.50\text{ eV}$ .

### A. Low-temperature emission of $\text{GaAs}_{1-x}\text{Bi}_x$ SQWs

Figs. 1(a)–1(d) show the normalized TRPL spectra for  $\text{GaAs}_{1-x}\text{Bi}_x$  SQWs with different Bi contents of  $x = 1.1\%$ ,

TABLE I. Growth parameters of  $\text{GaAs}_{1-x}\text{Bi}_x/\text{GaAs}$  SQWs. The Bi content and the QW width are determined by high-resolution X-ray diffraction.

Sample	Substrate temperature (°C)	As flux ( $10^{-8}$ millibars)	Bi flux ( $10^{-8}$ millibars)	Bi content (%)	QW width (nm)
#1	365	14	1.70	1.1	12
#2	280	25	1.70	6.0	14
#3	320	25	1.70	5.5	12
#4	300	11	0.42	2.1	13

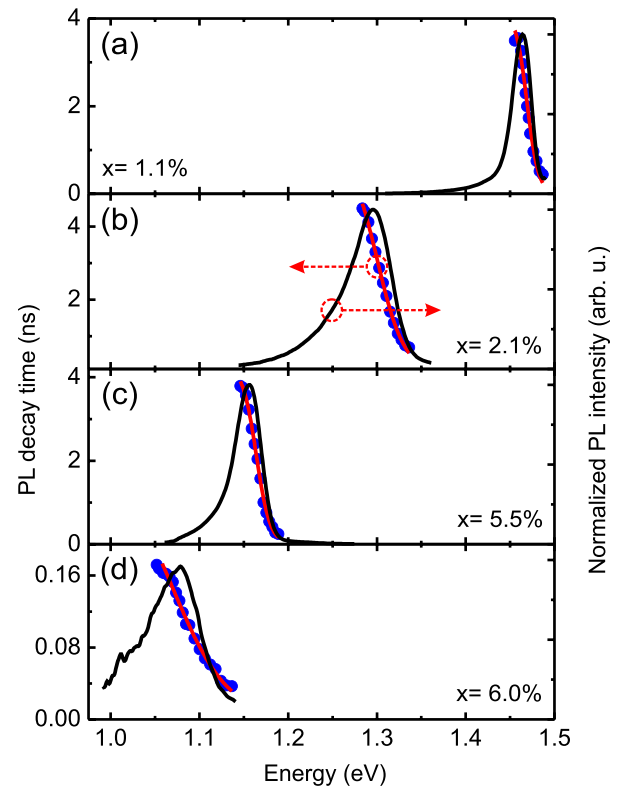


FIG. 1. TRPL spectra for  $\text{GaAs}_{1-x}\text{Bi}_x/\text{GaAs}$  SQWs with Bi contents of (a)  $1.1\%$ , (b)  $2.1\%$ , (c)  $5.5\%$ , and (d)  $6.0\%$ , measured under an excitation density of  $12.4\text{ MW/cm}^2$  at  $11\text{ K}$ . The blue circles in (a)–(d) show the PL decay time as a function of the emission energy. The solid red lines are the fits generated using Eq. (2).

$2.1\%$ ,  $5.5\%$ , and  $6.0\%$ , respectively, obtained at an excitation density of  $12.4\text{ MW/cm}^2$  for a lattice temperature of  $11\text{ K}$ . The corresponding normalized PL transients are plotted in Fig. 2. As expected, the PL spectra shift towards the low energy side with increasing Bi content. This reflects the band-gap shrinkage due to the valence-band anti-crossing interaction.<sup>2</sup> Based on the linear fit plotted in Fig. 3, the absolute slope of the band gap narrowing versus the Bi content is  $69 \pm 9\text{ meV}/\% \text{Bi}$  with respect to the band gap of GaAs. The slope is reduced by about  $10\%$  if the excitation density is increased by a factor of  $10$ . This value is in a reasonable agreement with previously reported ones.<sup>3,8,14</sup>

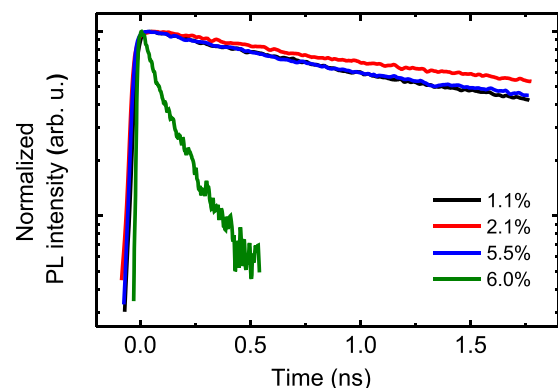


FIG. 2. Normalized PL transients of  $\text{GaAs}_{1-x}\text{Bi}_x/\text{GaAs}$  SQWs with  $x = 1.1\%$ ,  $2.1\%$ ,  $5.5\%$ , and  $6.0\%$ , obtained at an excitation density of  $12.4\text{ MW/cm}^2$  at  $11\text{ K}$ .

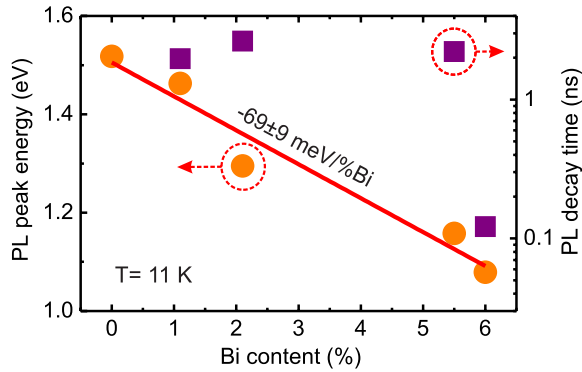


FIG. 3. PL peak energy and the PL decay time as a function of Bi content. The solid red line represents a linear fit to the data points of PL peak energy with respect to the band gap of GaAs.

In addition, all PL spectra display a similar asymmetric form with an exponential character of the low energy flank. The latter is attributed to the recombination of the electron-hole pairs trapped in localized states, which typically have an exponential density distribution.<sup>15,20</sup> As mentioned above, the presence of the localized states in the ternary semiconductor alloy Ga(AsBi) is attributed to an inhomogeneous distribution of Bi atoms and the existence of Bi clusters within the alloy structure, resulting in a broadening of the PL spectrum.<sup>6,12</sup> In the present case of a QW, well width and/or strain fluctuations can lead to localized states.<sup>21</sup> However, it is clearly visible that no clear correlation between the PL linewidth and the Bi content is observed. Moreover, the increased Bi content in GaAs<sub>1-x</sub>Bi<sub>x</sub> SQWs has a weak influence on the PL transients up to  $x=5.5\%$ . Yet, it becomes significantly faster when the Bi content is raised to 6.0%, as shown in Fig. 2. On the other hand, the PL decay time is reduced more than 10 times when the Bi content is increased from 5.5% to 6.0%, cf. Fig. 3. These points will be discussed in more detail in the following subsections.

## B. Excitation dependence of TRPL

Next, the dependence of the excitation density on the TRPL spectra and PL transients at 11 K is studied. The PL peak energy and the PL linewidth are shown as a function of the excitation density in Figs. 4(a) and 4(b), respectively. For all samples, the PL peak energy shifts significantly towards higher energies as the excitation density is increased up to 177 MW/cm<sup>2</sup>. For higher excitation densities, the PL peak energy is almost constant. In contrast, the PL linewidth varies only slightly between 1.77 MW/cm<sup>2</sup> and 17.7 MW/cm<sup>2</sup>. Then, it strongly increases when the excitation density is increased further. The blue-shift of the PL peak energy is attributed to the population of the localized states. This effect saturates at higher excitation densities.<sup>22</sup> The broadening of the PL spectra, however, is mainly affected by the occupation of higher confined states of the QW at increased excitation densities. These states are clearly observed as distinct peaks on the high-energy flank of the PL spectra, exemplary shown for the SQW with  $x=5.5\%$  in the inset of Fig. 4(b). A similar behavior has been reported by Mazur *et al.*<sup>10</sup> One also observes for the  $x=5.5\%$  sample that the PL peak energy

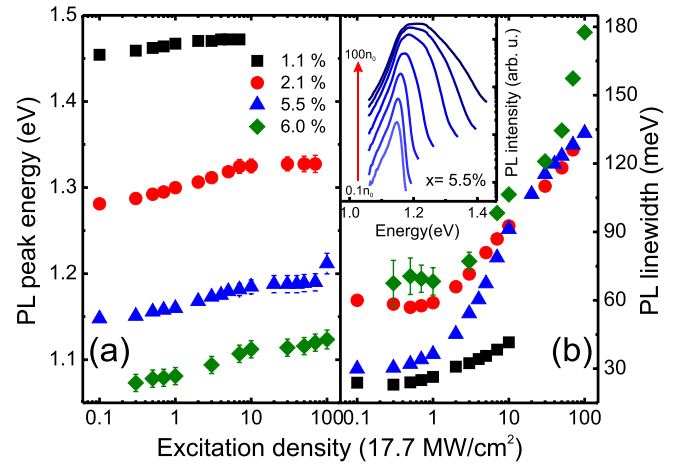


FIG. 4. (a) The PL peak energy and (b) the PL linewidth of GaAs<sub>1-x</sub>Bi<sub>x</sub>/GaAs SQWs as a function of excitation density at 11 K. The inset in (b) illustrates the PL spectra of the sample with  $x=5.5\%$  under different excitation densities of 0.1  $n_0$ , 0.3  $n_0$ ,  $n_0$ , 3  $n_0$ , 10  $n_0$ , 30  $n_0$ , and 100  $n_0$ , where  $n_0$  corresponds to the excitation density of 17.7 MW/cm<sup>2</sup>.

shifts abruptly from 1.18 to 1.22 eV at the excitation density of 1770 MW/cm<sup>2</sup> as the second confined state of the QW becomes the dominant emission channel. It should also be noted that due to the small band gap difference of about 55 meV between the GaAs barrier and the SQW with  $x=1.1\%$ , the overall PL spectrum is almost completely dominated by the barrier emission at excitation densities above 177 MW/cm<sup>2</sup>. In this regime, the peak of the PL emission from the QW cannot be unambiguously determined.

The PL decay time and the integrated PL intensity versus the excitation density are presented in Figs. 5(a) and 5(b), respectively. A considerable shortening of the PL decay time by about one order of magnitude is observed when the excitation density is increased by three orders of magnitude. However, the integrated PL intensity develops linearly with the excitation density and becomes sublinear at high excitation densities. In particular, the integrated PL intensity ( $I_{PL}$ ) as a function of the excitation intensity ( $I_{exc}$ ) is analyzed using the power-law,<sup>23</sup>

$$I_{PL} \propto I_{exc}^{\alpha} \quad (1)$$

The solid lines in Fig. 5(b) refer to the fits using Eq. (1). The dependence of  $I_{exc}$  on  $I_{PL}$  can be clearly discussed in two regimes for the four SQWs. As the  $I_{exc}$  is increased up to 177 MW/cm<sup>2</sup>, the values of  $\alpha_1$  are 0.90, 1.05, and 1.27 for the SQWs with  $x=2.1\%$ , 5.5%, and 6.0%, respectively. On the other hand,  $\alpha_1=1.15$  for  $x=1.1\%$ , as the  $I_{exc}$  increased up to 35.4 MW/cm<sup>2</sup>. Secondly, by the further increase of  $I_{exc}$ ,  $\alpha_2=0.40$ , 0.22, 0.33, and 0.80 for the samples with  $x=1.1\%$ , 2.1%, 5.5%, and 6.0%, respectively. As shown in Fig. 5(a), the decrease of the PL decay time with increasing  $I_{exc}$  in the first regime is attributed to the dominance of the recombination of the electron-hole pairs trapped in the localized states, resulting in a nearly linear increase of  $I_{PL}$  as the  $\alpha_1$ 's are approximately one. This behavior has already been discussed often in the literature.<sup>13,24-26</sup>

When non-radiative processes are efficiently involved at low temperature, a decrease of the carrier lifetime should be

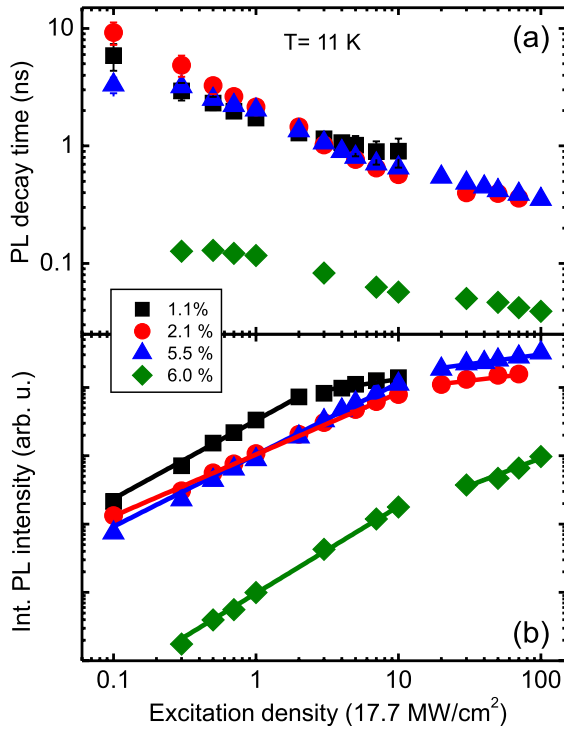


FIG. 5. Excitation density dependence of (a) the PL decay time and (b) the integrated PL intensity of GaAs<sub>1-x</sub>Bi<sub>x</sub>/GaAs SQWs measured at 11 K. The solid lines in (b) indicate the fits obtained using Eq. (1).

accompanied with a sublinear behavior of the PL intensity. This is indeed the case for even higher excitation densities. A decreasing decay time of PL together with a sublinear increase of  $I_{PL}$ , reflected in values of  $\alpha_2$  significantly lower than one, is attributed to an increasing contribution from capture processes into defect states as the carriers become delocalized and thus more mobile. Also, further contributions from Auger recombination processes<sup>27</sup> or heating effects are possible.<sup>24</sup>

**C. Temperature dependent PL spectra**

Fig. 6(a) shows the temperature evolution of the PL peak energy for the four investigated samples, taken under a relatively low CW-excitation density of 8 W/cm<sup>2</sup> to prevent any saturation of the localized states. The corresponding PL spectra of the SQW with  $x = 5.5\%$ , measured at various temperatures in a range from 10 K up to RT are represented in Fig. 6(b). For all samples, the PL peak energy exhibits a non-monotonous temperature dependence, the so-called S-shape.<sup>18,19,24</sup> This behavior is interpreted as follows: at very low temperatures, the PL emission arises primarily from the recombination of the electron-hole pairs trapped in the shallow localized states. The carriers can hop between the localized states via phonon-assisted tunnelling, recombine radiatively, or non-radiatively via defect states.<sup>28</sup> When the temperature is increased, the carriers are able to perform hopping transitions upward in energy, overcome local potential barriers, and are thus able to reach localized states that are even lower in energy.<sup>20</sup> Therefore, the PL energy peak initially shifts toward lower energies. At higher temperatures the carriers become more and more delocalized and the PL

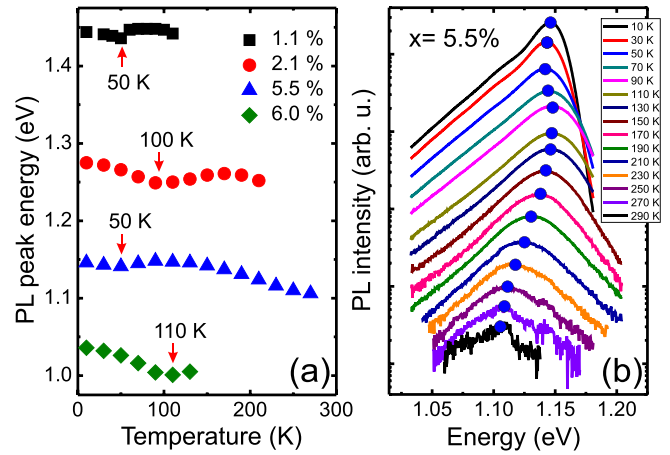


FIG. 6. The temperature dependence of (a) PL peak energy for the four investigated samples and (b) PL spectra for the SQW with  $x = 5.5\%$ , taken under a CW excitation density of 8 W/cm<sup>2</sup>. The closed blue circles are positioned in (b) to mark the temperature evolution of the PL peak energy.

peak energy shifts toward higher energies, due to the thermal depopulation of the band-tail states. For even higher temperatures, the majority of carriers are delocalized, at least with respect to the lowest of the energy scales of the potential fluctuations,<sup>6,20</sup> which will be discussed in Subsection III E. Ultimately, the PL peak energy exhibits a pronounced red-shift, related to the typical temperature-induced decrease of the band gap energy.<sup>29,30</sup>

For the further understanding of the carrier recombination mechanism, temperature dependent TRPL measurements are performed for all SQWs. Figs. 7(a) and 7(b) show the PL decay time and the integrated PL intensity as a function of temperature for an excitation density of 35.4 MW/cm<sup>2</sup>, respectively. A strong decrease of the PL

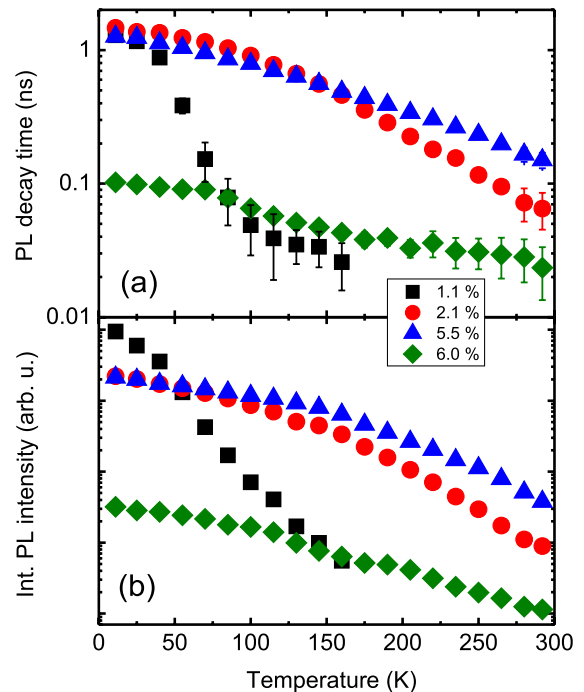


FIG. 7. (a) The PL decay time and (b) the integrated PL intensity of GaAs<sub>1-x</sub>Bi<sub>x</sub>/GaAs SQWs as a function of temperature measured under the excitation density of 35.4 MW/cm<sup>2</sup>.

intensity, accompanied by a shortening of the PL decay time is observed for all SQWs when the temperature is increased from 11 K to RT. The sample with the lowest Bi content shows, however, an even stronger decline of the PL intensity as well as the PL decay time already in the temperature range below 100 K. The PL intensity related to the SQW with  $x = 2.1\%$  ( $x = 5.5\%$  as well) decreases slowly with increasing temperature up to a certain point of 150 K and then drops fast. Also, the PL decay times in these samples are relatively long with values of around 1.5 ns and 1.2 ns for 2.1% and 5.5%, respectively. However, as the temperature is increased beyond 90 K, the PL decay decreases significantly to about 0.06 ns and 0.15 ns for 2.1% and 5.5% at RT, respectively. Furthermore, the PL intensity decreases by almost one order of magnitude when the Bi content is raised from 5.5% to 6.0% over the whole temperature range. A very short PL decay time of about 0.1 ns is observed at 11 K for the SQW with  $x = 6.0\%$ . In addition, the PL decay time is reduced by less than one order of magnitude when the temperature is increased up to RT. The decrease of the decay time is accompanied by the quenching of the PL intensity. Thus, the shortening of the decay time is mainly associated with the competition between radiative and non-radiative processes. In particular, radiative recombination of localized carriers is expected to contribute significantly to the decay dynamics at low temperatures leading to a rather slow decay. For higher temperatures, as non-radiative channels are thermally activated,<sup>31,32</sup> the decay time decreases. Furthermore, the rapid degradation of the PL intensity as well as the PL decay time for the SQW with  $x = 1.1\%$  is again attributed to the small band gap offset between the barrier and QW. In detail, the photo-generated carriers in the QW are thermally activated and escape via GaAs barrier. Moreover, the dramatic decrease of the PL intensity as well as the corresponding decay time for the SQW with  $x = 6.0\%$ , in comparison to the other SQWs, reflects an increased emergence of structural defects and subsequent degradation of the material quality of the QW.<sup>12</sup> In other words, the increased amount of the non-radiative centers leads to a decreased PL efficiency.

#### D. Emission energy dependence of the PL decay time

In order to characterize the distribution of the localized states in GaAs<sub>1-x</sub>Bi<sub>x</sub>/GaAs SQWs, the emission energy dependence of the PL decay time is studied. The PL decay times versus the emission energy for the four SQWs are shown as blue circles in Figs. 1(a)–1(d), taken at a temperature of 11 K and an excitation density of 12.4 MW/cm<sup>2</sup>. The PL decay times are determined from the spectrally integrated PL transients across  $\pm 5$  meV. A large increase in the PL decay time with decreasing energy is clearly observed for all of the samples as well. For the low emission energies of the PL spectrum, the radiative recombination is predominant due to strongly localized electron-hole pairs.<sup>33</sup> At the high energy side of the PL spectrum, the carriers also perform tunneling transitions toward the lower energies which lead to a shorter decay time of the PL.<sup>5,34</sup>

The PL decay time as a function of the emission energy is analyzed using the Gourdon and Lavallard model,<sup>34</sup> which

includes the mechanisms for the recombination as well as the aforementioned relaxation of the charge carriers toward lower energies. According to this model, the density of states is assumed to be exponential, proportional to  $e^{\frac{E-E_0}{E_0}}$  with a characteristic energy ( $E_0$ ). Hence, the PL decay times as a function of the emission energy are fitted by

$$\tau_{PL}(E) = \frac{\tau_{rec}}{1 + e^{\frac{E-E_{me}}{E_0}}}, \quad (2)$$

where  $\tau_{rec}$  indicates the recombination lifetime and  $E_{me}$  is the energy at which the relaxation rate of an electron-hole pair toward lower-lying localized states and the recombination rate are equal.<sup>34</sup> In this context,  $E_{me}$  plays a similar role as the mobility edge. The solid red lines in Figs. 1(a)–1(d) are obtained from the fit to the measured  $\tau_{rec}$  data using Eq. (2). The obtained fitting parameters of the  $\tau_{rec}$  together with  $E_{me}$  are summarized in Fig. 8(a) and  $E_0$  (green circles) in Fig. 8(b) as a function of Bi content. The mobility edge

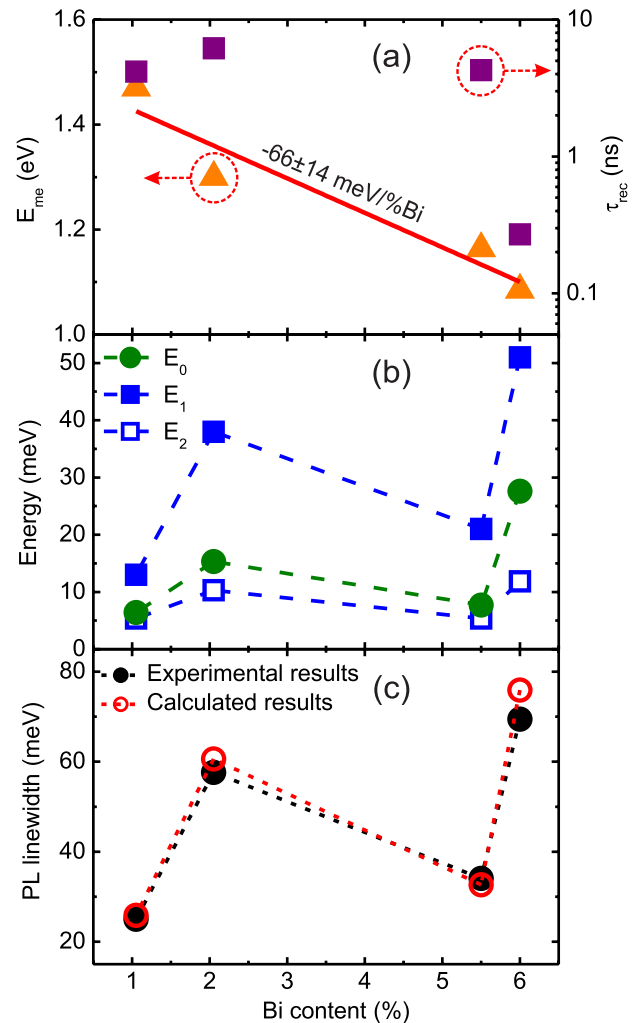


FIG. 8. The dependence of (a) the recombination lifetime  $\tau_{rec}$  and the mobility edge  $E_{me}$ ; (b) the energy scales  $E_0$ ,  $E_1$ , and  $E_2$ ; and (c) the PL linewidth on the Bi content. The values of  $\tau_{rec}$ ,  $E_{me}$ , and  $E_0$  are determined using Eq. (2).  $E_1$  and  $E_2$  are estimated according to the double energy scales model. The circles in (c) indicate the variation of the PL linewidth; the black closed ones are determined from PL spectra measured under the excitation density of 12.4 MW/cm<sup>2</sup> at 11 K, and the red open ones are extracted using Eq. (6).

decreases linearly with increasing Bi content, reflecting the narrowing of the band-gap energy. The reduction rate of  $E_{me}$  is  $-64 \pm 14$  meV/%Bi, which is in a good agreement with the decrease of the PL peak energy. The  $\tau_{rec}$  exhibits an analogous behavior as the overall PL decay time. Up to  $x=5.5\%$ , the  $\tau_{rec}$  is relatively long, and then it strongly shortens by more than one order of magnitude for the SQW with  $x=6.0\%$ . The obtained values of  $E_0$  are 6.4, 15.3, 7.7, and 26.7 meV for  $x=1.1\%$ , 2.1%, 5.5%, and 6.0%, respectively. The variation of  $E_0$  shows a significant fluctuation with a slight tendency to increase with Bi content. The relatively small values of  $E_0$  reflect that the carrier dynamics at very low temperature and low excitation condition are affected by the potential disorder associated essentially with Bi clusters.<sup>5</sup> Furthermore, a similar behavior of both  $E_0$  and the PL linewidth versus Bi content is obviously observed in Figs. 8(b) and 8(c), respectively. The latter demonstrates the fact that the broadening of the PL spectrum is related mainly to the density of the localized states in the low energy band tail of the PL spectrum.

### E. Two energy scales model

For the interpretation of the specific features of the PL spectra of  $\text{GaAs}_{1-x}\text{Bi}_x/\text{GaAs}$  SQWs, we employ a model with double energy scales.<sup>20</sup> The long-range disorder scale ( $E_1$ ) is attributed to the potential compositional fluctuations<sup>20</sup> and/or the possible imperfect interfaces between the QW and the barriers,<sup>21</sup> whereas the short-range disorder scale ( $E_2$ ) arises from the presence of Bi clusters<sup>6</sup> as well as the short range compositional fluctuations within the alloy structure. According to the proposed model, an exponential distribution of the localized states is assumed. The density of the localized states is given by

$$g(E) = \frac{N_0}{E_1 - E_2} (e^{\frac{E}{E_1}} - e^{\frac{E}{E_2}}), \quad (3)$$

where  $N_0$  is the concentration of the localized states. Experimentally,  $E_1$  relates to the energy distribution of the localized states at low temperatures under low excitation intensities and is determined from the logarithmical slope  $\beta$  of the low energy flank of the PL spectrum as follows:

$$E_1 = \frac{1}{\beta}. \quad (4)$$

On the other hand,  $E_2$  is extracted using Eq. (5) with respect to the temperature ( $T_{st}$ ) at which the PL peak energy has its local minimum within the above-monitored S-shape.  $T_{st}$  indicates also the maximum of the Stokes shift, i.e., the energetic difference between the absorption edge and the PL emission maximum,<sup>35</sup>

$$k_B T_{st} = (0.75 \div 0.80) E_2, \quad (5)$$

where  $k_B$  is the Boltzmann constant. The values of  $T_{st}$  are 50, 100, 50, and 110 K for the SQWs with  $x=1.1\%$ , 2.1%, 5.5%, and 6.0%, respectively. The two characteristic energy scales  $E_1$  and  $E_2$ , evaluated using the trends of the above-mentioned

experimental observation of the studied SQWs, are summarized in Fig. 8(b). The long energy scale  $E_1$  is estimated to be about 25, 58, 34, and 69 meV and the short one  $E_2$  to be about 5, 10, 5, and 12 meV for  $x=1.1\%$ , 2.1%, 5.5%, and 6.0%, respectively. Ultimately, the low-temperature PL linewidth ( $FWHM_0$ ) under low excitation conditions is calculated according to the present model using the relation,

$$FWHM_0 = 0.85E_1 + 2.75E_2. \quad (6)$$

The obtained values of the  $FWHM_0$  for the investigated structures are compared to the experimental ones taken at 11 K in Fig. 8(c). An excellent agreement is obtained between the measured PL linewidth and the estimation based on the analysis of the disorder scales. Similar to the above discussion on the variation in the characteristic energy scale  $E_0$ , derived from the Gourdon and Lavallard model,  $E_1$  and  $E_2$  behave similar with increasing Bi content, and obviously follow the PL linewidth, cf. Fig. 8(c). In spite of the intuitive thought that the energy scales of disorder potential have to increase with the concentration of the fluctuating compositional component, e.g., the In content in  $\text{In}_x\text{Ga}_{1-x}\text{N}$  MQWs,<sup>36</sup> a decrease of these scales is reported for the GaNAsP MQWs when the N content is increased.<sup>37</sup> However, in the case of  $\text{GaAs}_{1-x}\text{Bi}_x/\text{GaAs}$  SQWs the energy scales show a weak dependence of the Bi content. The fluctuation of both  $E_1$  and  $E_2$  with increasing Bi content indicates that the density of the localized states broadens differently for each sample. On the other hand, the low values of the energy scales for the SQW with a relatively high Bi content of 5.5% indicate a comparatively weak disorder potential and good optical properties of this particular sample. This is indeed desirable for long wavelength applications. Since the disorder effects are essentially related to the growth conditions, the performance of the optoelectronic devices would be enhanced if these conditions are optimized specifically.

### IV. CONCLUSION

The impact of Bi content on the localization effects and the carrier dynamics in  $\text{GaAs}_{1-x}\text{Bi}_x/\text{GaAs}$  SQWs, with  $x=1.1\%$ , 2.1%, 5.5%, and 6.0%, is studied by means of CW- and TRPL. A linear reduction in the band gap occurs with Bi incorporation into GaAs at a rate of  $69 \pm 9$  meV/%Bi with respect to the band gap of GaAs. At low temperatures, a substantial increase in the PL decay time with decreasing emission energy is observed under low excitation power densities. The temperature dependence of the PL peak energy shows a non-monotonous S-shape behavior, which is interpreted by supposing that the localized carriers exhibit hopping transitions between the localized states. In addition, the PL exhibits a typical thermal quenching as well as a significant shortening of the decay time due to the delocalization of carriers and increased non-radiative recombination. Moreover, the drastic reduction of the PL efficiency for the SQW with  $x=6.0\%$  is ascribed to the large increase of the defects within the QW structure. Also, the rapid degradation of the PL emission for the SQW with  $x=1.1\%$  is interpreted,

due to the small band gap offset between the barrier and the quantum well. Two theoretical models are used to quantify the disorder parameters. A straightforward model with a single energy scale is based on the carrier dynamics at low temperatures. It takes into account the transfer of excitons to the low energy tail states. The second model describes the hopping of excitons with two energy scales. One scale is attributed to disorder effects caused by the long range potential fluctuation associated with the Bi content or/and geometrical imperfections across the interfaces between the QW and the barriers. The second is ascribed to the presence of Bi clusters and short range fluctuations within the alloy structure. Our results demonstrate that the characteristic energy scales change in a similar way as a Bi content is varied. However, a considerable fluctuation for the energy scales is observed with a slight trend to increase with Bi content. Interestingly, our findings indicate a weak disorder potential for a sample with a relatively high Bi content of 5.5%.

## ACKNOWLEDGMENTS

The Marburg Group gratefully acknowledges financial support through the Research Training Group 1782-Functionalization of Semiconductors by the German Science Foundation (DFG).

- <sup>1</sup>S. Francoeur, M.-J. Seong, A. Mascarenhas, S. Tixier, M. Adamcyk, and T. Tiedje, *Appl. Phys. Lett.* **82**, 3874 (2003).
- <sup>2</sup>K. Alberi, O. D. Dubon, W. Walukiewicz, K. M. Yu, K. Bertulis, and A. Krotkus, *Appl. Phys. Lett.* **91**, 051909 (2007).
- <sup>3</sup>B. Fluegel, S. Francoeur, A. Mascarenhas, S. Tixier, E. C. Young, and T. Tiedje, *Phys. Rev. Lett.* **97**, 067205 (2006).
- <sup>4</sup>A. Chernikov, V. Bornwasser, M. Koch, S. W. Koch, X. Lu, S. R. Johnson, D. A. Beaton, T. Tiedje, and S. Chatterjee, *Semicond. Sci. Technol.* **27**, 085012 (2012).
- <sup>5</sup>S. Imhof, C. Wagner, A. Thränhardt, A. Chernikov, M. Koch, N. S. Koster, S. Chatterjee, S. W. Koch, O. Rubel, X. Lu, S. R. Johnson, D. A. Beaton, and T. Tiedje, *Appl. Phys. Lett.* **98**, 161104 (2011).
- <sup>6</sup>S. Imhof, A. Thränhardt, A. Chernikov, M. Koch, N. S. Koster, K. Kolata, S. Chatterjee, S. W. Koch, X. Lu, S. R. Johnson, D. A. Beaton, T. Tiedje, and O. Rubel, *Appl. Phys. Lett.* **96**, 131115 (2010).
- <sup>7</sup>K. Oe and H. Okamoto, *Jpn. J. Appl. Phys., Part 2* **37**, L1283 (1998).
- <sup>8</sup>S. Tixier, M. Adamcyk, T. Tiedje, S. Francoeur, A. Mascarenhas, P. Wei, and F. Schiettekatte, *Appl. Phys. Lett.* **82**, 2245 (2003).
- <sup>9</sup>X. Lu, D. A. Beaton, R. B. Lewis, T. Tiedje, and Y. Zhang, *Appl. Phys. Lett.* **95**, 041903 (2009).
- <sup>10</sup>Y. I. Mazur, V. G. Dorogan, M. Schmidbauer, G. G. Tarasov, S. R. Johnson, X. Lu, S.-Q. Yu, Zh. M. Wang, T. Tiedje, and G. J. Salamo, *Nanotechnology* **22**, 375703 (2011).
- <sup>11</sup>Y. Tominaga, Y. Kinoshita, G. Feng, K. Oe, and M. Yoshimoto, *Phys. Status Solidi C* **5**, 2719 (2008).
- <sup>12</sup>A. R. Mohmad, F. Bastiman, C. J. Hunter, J. S. Ng, S. J. Sweeney, and J. P. R. David, *Appl. Phys. Lett.* **99**, 042107 (2011).
- <sup>13</sup>A. R. Mohmad, F. Bastiman, J. S. Ng, S. J. Sweeney, and J. P. R. David, *Appl. Phys. Lett.* **98**, 122107 (2011).
- <sup>14</sup>V. V. Pačebutas, K. Bertulis, G. Aleksejenko, and A. Krotkus, *J. Mater. Sci.: Mater. Electron.* **20**, S363 (2009).
- <sup>15</sup>I. A. Buyanova, W. M. Chen, and C. W. Tu, *Solid-State Electron.* **47**, 467 (2003).
- <sup>16</sup>P. Benalloul, J. Benoit, R. Mach, G. O. Müller, and G. U. Reinsperger, *J. Cryst. Growth* **101**, 989 (1990).
- <sup>17</sup>X. Chen, B. Henderson, and K. P. O'Donnell, *Appl. Phys. Lett.* **60**, 2672 (1992).
- <sup>18</sup>A. Kaschner, J. Holst, U. von Gfug, A. Hoffmann, F. Bertram, T. Riemann, D. Rudloff, P. Fischer, J. Christen, R. Aeverbeck, and H. Riechert, *1999 MRS Fall Meeting-Symposium W-GaN and Related Alloys*, edited by H. Amano, R. Feenstra, T. Myers, and M. S. Shur (Mater. Res. Soc. Symp. Proc., 1999), Vol. 595, p. F99W11.34.
- <sup>19</sup>Y.-H. Cho, G. H. Gainer, A. J. Fischer, J. J. Song, S. Keller, U. K. Mishra, and S. P. DenBaars, *Appl. Phys. Lett.* **73**, 1370 (1998).
- <sup>20</sup>K. Jandieri, C. Jurecka, J. Ohlmann, A. Beyer, B. Kunert, S. D. Baranovskii, K. Volz, W. Stolz, and F. Gebhard, *Phys. Status Solidi C* **8**, 163 (2011).
- <sup>21</sup>L. Grenouillet, C. Bru-Chevallier, G. Guillot, P. Gilet, P. Duvaut, C. Vannuffel, A. Million, and A. Chenevas-Paule, *Appl. Phys. Lett.* **76**, 2241 (2000).
- <sup>22</sup>F. Ishikawa, Á. Guzmán, O. Brandt, A. Trampert, and K. H. Ploog, *J. Appl. Phys.* **104**, 113502 (2008).
- <sup>23</sup>X. Zhongying, X. Jizong, G. Weikun, Z. Baozhen, X. Junying, and L. Yuzhang, *Solid State Commun.* **61**, 707 (1987).
- <sup>24</sup>R. Kudrawiec, M. Syperek, P. Poloczek, J. Misiewicz, R. H. Mari, M. Shafi, M. Henini, Y. G. Gobato, S. V. Novikov, J. Ibanez, M. Schmidbauer, and S. I. Molina, *J. Appl. Phys.* **106**, 023518 (2009).
- <sup>25</sup>N. A. Riordan, C. Gogineni, S. R. Johnson, X. Lu, T. Tiedje, D. Ding, Y.-H. Zhang, R. Fritz, K. Kolata, S. Chatterjee, K. Volz, and S. W. Koch, *J. Mater. Sci.: Mater. Electron.* **23**, 1799 (2012).
- <sup>26</sup>Yu. I. Mazur, V. G. Dorogan, M. Schmidbauer, G. G. Tarasov, S. R. Johnson, X. Lu, M. E. Ware, S.-Q. Yu, T. Tiedje, and G. J. Salamo, *J. Appl. Phys.* **113**, 144308 (2013).
- <sup>27</sup>V. Pačebutas, R. Butkutė, B. Čechavičius, J. Kavaliauskas, and A. Krotkus, *Thin Solid Films* **520**, 6415 (2012).
- <sup>28</sup>M. Urban, H. Schwab, and C. Klingshirn, *Phys. Status Solidi B* **166**, 423 (1991).
- <sup>29</sup>Y. P. Varshni, *Physica* **34**, 149 (1967).
- <sup>30</sup>P. Lautenschlager, M. Garriga, and M. Cardona, *Phys. Rev. B* **36**, 4813 (1987).
- <sup>31</sup>O. Rubel, S. D. Baranovskii, K. Hantke, W. W. Ruhle, P. Thoma, K. Volz, and W. Stolz, *Phys. Rev. B* **73**, 233201 (2006).
- <sup>32</sup>C. Netzel, V. Hoffmann, T. Wernicke, A. Knauer, M. Weyers, M. Kneissl, and N. Szabo, *J. Appl. Phys.* **107**, 033510 (2010).
- <sup>33</sup>R. A. Mair, J. Y. Lin, H. X. Jiang, E. D. Jones, A. A. Allerman, and S. R. Kurtz, *Appl. Phys. Lett.* **76**, 188 (2000).
- <sup>34</sup>C. Gourdon and P. Lavallard, *Phys. Status Solidi B* **153**, 641 (1989).
- <sup>35</sup>F. Yang, M. Wilkinson, E. J. Austin, and K. P. O'Donnell, *Phys. Rev. Lett.* **70**, 323 (1993).
- <sup>36</sup>K. Kazlauskas, G. Tamulaitis, P. Pobedinskas, A. Žukauskas, M. Springis, C. F. Huang, Y. C. Cheng, and C. C. Yang, *Phys. Rev. B* **71**, 085306 (2005).
- <sup>37</sup>K. Jandieri, M. K. Shakfa, S. Liebich, M. Zimprich, B. Kunert, C. Karcher, A. Chernikov, K. Volz, W. Stolz, M. Koch, S. Chatterjee, W. Heimbrodt, F. Gebhard, and S. D. Baranovskii, *Phys. Rev. B* **86**, 125318 (2012).